SLAC-PUB-95-7004
August 1995

The Lifetime Probability Tag Measurement of R_b using the SLD

The SLD Collaboration [1]

Stanford Linear Accelerator Center
Stanford University
Stanford, CA 94309

ABSTRACT

We present a new measurement of $R_b = \Gamma_{Z^o \to b\bar{b}}/\Gamma_{Z^o \to hadrons}$ using a lifetime double tag on 150k hadronic Z^o events collected from the SLD 1993 and 1994 runs. The method utilizes the high precision 3-D position measurements provided by the CCD vertex detector and the small stable SLC beams to obtain a b hemisphere tagging efficiency of 31% for a purity of 94%. The b-hemisphere tagging efficiency is measured from the data reducing dependence on the B-decay model and detector simulation. We obtain a result of $R_b = 0.2171 \pm 0.0040_{statistical} \pm 0.0037_{systematic} \pm 0.0023_{R_c}$.

Presented at the *International Europhysics Conference on High-Energy Physics (HEP 95)*, Brussels, Belgium, July 27-August 2, 1995.

[1]This work was supported by Department of Energy contracts: DE-FG02-91ER40676 (BU), DE-FG03-92ER40701 (CIT), DE-FG03-91ER40618 (UCSB), DE-FG03-92ER40689 (UCSC), DE-FG03-93ER40788 (CSU), DE-FG02-91ER40672 (Colorado), DE-FG02-91ER40677 (Illinois), DE-AC03-76SF00098 (LBL), DE-FG02-92ER40715 (Massachusetts), DE-AC02-76ER03069 (MIT), DE-FG06-85ER40224 (Oregon), DE-AC03-76SF00515 (SLAC), DE-FG05-91ER40627 (Tennessee), DE-AC02-76ER00881 (Wisconsin), DE-FG02-92ER40704 (Yale); National Science Foundation grants: PHY-91-13428 (UCSC), PHY-89-21320 (Columbia), PHY-92-04239 (Cincinnati), PHY-88-17930 (Rutgers), PHY-88-19316 (Vanderbilt), PHY-92-03212 (Washington); the UK Science and Engineering Research Council (Brunel and RAL); the Istituto Nazionale di Fisica Nucleare of Italy (Bologna, Ferrara, Frascati, Pisa, Padova, Perugia); and the Japan-US Cooperative Research Project on High Energy Physics (Nagoya, Tohoku).

1 Introduction

Significant top mass dependent radiative corrections to the cross-section for $Z^0 \to b\bar{b}$ are expected. In this cross-section, the vertex corrections are obscured by oblique corrections(loop corrections to the propagator). The vertex corrections may be isolated by taking the ratio of the $Z^0 \to b\bar{b}$ cross-section to other cross-sections for hadronic decays of the Z^0. In these ratios the oblique corrections mostly cancel while the vertex corrections remain. Experimentally, the best ratio to use is $\Gamma(Z^0 \to b\bar{b})/\Gamma(Z^0 \to hadrons)$. Most experimental uncertainties cancel in the ratio allowing possible new physics signals to be observed. Using the current top mass measurements from CDF($176 \pm 8 \pm 10\,\mathrm{GeV}/c^2$)[1] and D0($199^{+19}_{-21} \pm 22\,\mathrm{GeV}/c^2$)[2] one expects a change of ~ -1 to -2% in R_b from the massless top quark value of 0.2193[3]. LEP has made measurements of R_b using several techniques[9]. and their current average is 1.8σ high compared to the Standard Model[3]. It is therefore interesting to measure R_b with a separate experimental apparatus as part of the effort to achieve increased precision on this important measurement.

During the 1994 run of the SLAC Large Detector(SLD), 100K Z^0 decays were collected. This has allowed the use of a hemisphere b-tagging technique to obtain a more precise measurement of $R_b = \frac{\Gamma(Z^0 \to b\bar{b})}{\Gamma(Z^0 \to hadrons)}$. Hemispheres are b-tagged by cutting on the probability that the tracks within a hemisphere are consistent with coming from the primary vertex. The rates of tagging one and both hemispheres in an event are used to simultaneously measure the b-tagging efficiency and R_b. We begin by describing the experimental apparatus followed by details of the analysis and results obtained.

2 The SLAC Large Detector

Observations of the Z^0 decay products are made using the SLD. The detector components relevant to this analysis include: the liquid argon calorimeter(LAC) for measuring energy flow[7]; the central drift chamber(CDC) for charged track identification and momentum measurements[5]; and a CCD pixel vertex detector(VXD) for precise position measurements near the interaction point[6]. The tracking and calorimeter systems are used by the analysis presented here and will be briefly discussed.

The LAC consists of a barrel section covering $|\cos\theta| < 0.84$ and endcaps covering $0.82 < |\cos\theta| < 0.98$ for the full azimuthal range. The energy resolution of the calorimeter barrel for electromagnetic showers of energy E is $\frac{\sigma}{E} = \frac{15\%}{\sqrt{E(GeV)}}$ and $\frac{60\%}{\sqrt{E(GeV)}}$ for hadronic showers.

The tracking systems (CDC and VXD) provide impact parameter resolutions of 76 μm in the $r\phi$ view and 80 μm in the rz view for 1 GeV/c tracks at $\cos\theta = 0$. The impact parameter resolution for high momentum tracks is determined from the two track miss distance using $Z^0 \to \mu^+\mu^-$ events. The single track impact parameter resolution is found to be 11 μm in the $r\phi$ view and 38 μm in the rz view. The

momentum resolution for the combined CDC and VXD track fit is $\frac{\delta p_\perp}{p_\perp} = 0.01 \oplus 0.0026\, p_\perp$. Details of the SLD and tracking performance may be found in Ref. [8] and Ref. [4].

2.1 Event Selection

To decrease contamination from non-hadronic interactions and to ensure the relevant detector components are fully operational on a given event the following criteria are placed on events passing the event trigger. The visible energy in events as measured from charged tracks must exceed 18 GeV. The thrust axis, determined from calorimeter clusters, is required to be in $|cos\theta| < 0.71$ which is well within the VXD acceptance. At least 7 CDC tracks are required to be present to assist in eliminating $\gamma\gamma$ and $\tau^+\tau^-$ events. At least one CDC track must have hits from the first or second CDC layer to ensure that the high voltage to these layers is on. At least three tracks with two or more VXD hits must be found.

Data from the 1993 and 1994 SLD runs and corresponding Monte Carlo are used. To reduce the systematic uncertainty coming from the statistical uncertainty on the hemisphere correlation, extra $b\bar{b}$ samples were generated. A total of 71k data events, and from the Monte Carlo 142k $b\bar{b}$, 35K $c\bar{c}$, and 122k uds events passing the event selection are used for the analysis.

2.2 Track Selection

Poorly measured tracks and tracks resulting both from interactions with the detector material and from long lived particle decays often have large impact parameters that can lead to contamination of the b-tagging signal. These tracks are efficiently removed by requirements on the measured production point of the tracks and by identifying and removing long lived neutral particles that decay into a pair of tracks (V^0) before leaving the track detection region.

Well measured tracks are selected by requiring that the CDC track start at radius < 39.0 cm, and has > 40 hits. The CDC track is required to extrapolate to within 1 cm of the $\langle IP \rangle$ in xy, and within 1.5 cm of the PV in z to eliminate tracks from interaction with the detector material and poorly measured tracks. The fit of the CDC track must also satisfy $\chi^2/d.o.f. < 5$. At least one VXD hit is required, and the combined CDC/VXD fit must satisfy $\chi^2/d.o.f. < 5$. Tracks with xy impact parameter errors $> 250\ \mu$m, or with xy impact parameters > 3.0 mm with respect to the $\langle IP \rangle$ are removed. The impact parameter error cut acts both as a quality cut and an effective minimum momentum cut. The impact parameter cut assists in removing poorly measured tracks and long-lived strange particle decay products, gamma conversion and nuclear interaction products. A cut on the 3-D distance of closest approach of the track to the jet axis(δ_j) and on the distance from the primary vertex to the point on the jet at which the track is closest(P_j) are used. These quantities are illustrated in Fig. 1. A cut of 16σ on $\delta_{jet}/\sigma(\delta_{jet})$ and a cut of 5 cm on P_j results in 92% of the b decay tracks being kept but only 45% of the tracks from long lived particle decays still remain.

3 Tracking Efficiency and Resolution Corrections

The Monte Carlo is corrected to yield the proper fraction of quality tracks by systematically removing tracks according to the discrepancy between data and Monte Carlo on the fraction of CDC tracks classified as good and on the CDC to VXD linking rate for the good CDC tracks. The correction is performed by determining the difference between data and Monte Carlo on the quality track multiplicity fraction in ranges of $p_\perp$, $\cos\theta$, ϕ, and the angle with respect to jet direction for CDC tracks and in the difference in fraction of good CDC tracks that link to VXD hits in ranges of p, $\cos\theta$, and ϕ. About 4% of the Monte Carlo tracks are removed to correct for both the good CDC and linking fractions.

Tracks that appear not to come from the primary vertex can be eliminated from the impact parameter distributions. The resulting distribution is indicative of the convolution of the detector resolution and the primary vertex resolution. This distribution is called the negative impact parameter distribution. The negative impact parameter distribution from the data and the Monte Carlo are compared in the $r\phi$ and rz projections to determine the residual amount of resolution degradation to be applied to the Monte Carlo. The xy impact parameter distributions match well and no resolution corrections were required. In rz the width of the Gaussian degradation function needed to obtain the best match of the Monte Carlo core with the data was determined to be $\frac{20\mu m}{sin\theta}$. No adjustment for the non-Gaussian tail was required. Systematic ϕ dependent shifts of the track z at the xy point of closest approach (z_{doca}) with magnitudes typically around $\pm 20\mu m$ were observed in the data and are applied to the z_{doca} of the Monte Carlo tracks. After the resolution and efficiency corrections have been applied the comparison of the Monte Carlo and data for the significance variable, χ(see Sect. 4), is as shown in Fig. 3.

4 b-Tagging Procedure

The measurement is performed in a manner similar to that outlined by ALEPH[9]. To tag a hemisphere one starts by forming a probability that each track is consistent with coming from the primary vertex. This is done by using the minimized 3-D normalized impact parameters(χ) of the tracks. This quantity is signed negative if the 3-D point of closest approach between the track and the jet axis is behind the measured primary vertex position. A resolution function(R) is parameterized to fit the $-\chi$ distribution of tracks in Monte Carlo uds events. From this, the integral probability that a track is consistent with coming from the primary vertex position is determined. Then, these probabilities are combined to form the integral probability that the collection of tracks in a hemisphere are consistent with all coming from the primary vertex. A hemisphere is then tagged by requiring that the probability for the hemisphere is below a cut.

x_0=ϕ=azimuthal angle of momentum vector
x_1=k=$1/p_\perp$ = curvature
x_2=s=$tan(\lambda)$ = tangent of dip angle
x_3=ξ=$(POCA_x - PV_x)sin\phi - (POCA_y - PV_y)cos\phi$
x_4=η=(z at $POCA_{xy} - PV_z)cos\lambda$

Table 1: Track helix parameter definitions.

4.1 The Minimized 3-D Impact Parameter(χ)

The tag variable, χ, is effectively the minimal value obtained on the track trajectory for the quantity

$$\delta^{3D} = \sqrt{(\frac{x - x_{PV}}{\sigma_x})^2 + (\frac{y - y_{PV}}{\sigma_y})^2 + (\frac{z - z_{PV}}{\sigma_z})^2}$$

where (x, y, z) represent a position on the track trajectory, $(x, y, z)_{PV}$ represent the measured primary vertex position and $\sigma_{x,y,z}$ are the impact parameter uncertainties. Using the full 3-D information makes the tag variable a more sensitive measure of the lifetime. In this section, the procedure by which χ is determined, and the signing of χ will be described.

The tag variable, χ, is the contribution to the fit quality of a track from adding the primary vertex as an extra track hit with its corresponding position uncertainties. The uncertainty in the primary vertex position was determined from the individual procedures for measuring the xy and z of the primary vertex position described in Ref. [4]. The procedure for determining xy position uses an average over tracks in many hadronic events. The result is that there is no degradation of the xy position resolution for $b\bar{b}$ events compared to light flavor events. The z position is determined event to event from tracks consistent with the xy primary vertex position. The primary vertex position uncertainty is determined to be σ_{PV}= ($7\mu m$,$7\mu m$,$38\mu m$).

This is then used to modify the error matrix from the CDC+VXD track fit as follows:

$$\chi^2 = (\vec{m} - \vec{x})^\dagger V^{-1} (\vec{m} - \vec{x}) + x_3^2/\sigma_{\xi,\xi} + x_4^2/\sigma_{\eta,\eta} \quad (1)$$

where

- x=vector of new track parameters defined in Table 1.
- m=vector of original measured track parameters
- V^{-1}=inverse of the original track error matrix
- $\sigma_{\xi,\xi}$=variance of ξ from uncertainty in measured primary vertex position
- $\sigma_{\eta,\eta}$=variance of η from uncertainty in measured primary vertex position

$POCA_i$ and PV_i are the ith components of the $r\phi$ point of closest approach and primary vertex position respectively.

Next, the track parameters are recalculated using the new error matrix, which includes the primary vertex, by minimizing the χ^2 with respect to each parameter as follows:

$$\frac{\delta\chi^2}{\delta m} = 0 = m^\dagger V^{-1} - (x^\dagger V^{-1} + \xi/\sigma_{\xi,\xi} + \eta/\sigma_{\eta,\eta})$$

The new error matrix V^{-1}_{new} is: V^{-1} except

$$V^{-1}_{3,3new} = V^{-1}_{3,3} + 1/\sigma_{\xi,\xi} \quad and \quad V^{-1}_{4,4new} = V^{-1}_{4,4} + 1/\sigma_{\eta,\eta}$$

The new track parameters are then obtained from:

$$\vec{x} = V_{new} * V^{-1} \times \vec{m}$$

Once this has been done the χ^2 coming from the contribution of the primary vertex is calculated from Eqn. 1.

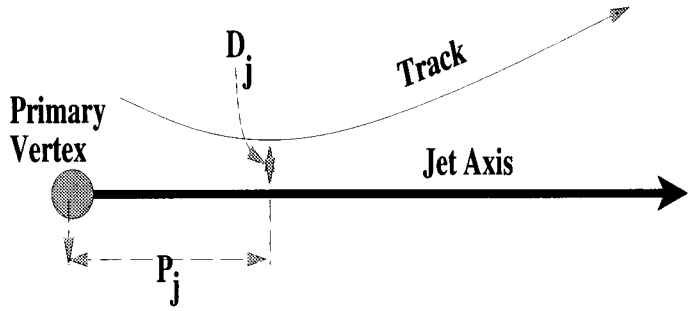

Figure 1: The signing of χ.

The χ is signed by whether the track passes closest to the jet axis it is associated with in front(positive) or behind(negative) the primary vertex. This is the sign of P_j in Fig. 1. The signed χ distributions for Monte Carlo and data are shown in Fig. 2.

4.2 Forming Track and Hemisphere Probabilities

From the χ for the track, the probability that the track is consistent with coming from background events is determined. This is accomplished by fitting the Monte Carlo *uds* distribution of χ to a resolution function as shown in Fig. 4. The resolution function($R(\chi)$) is formed from a factor of χ to account for phase space multiplied by Gaussians for describing the core and exponentials for describing the tails. The probability (P_{track}) that one will measure the same χ or worse is given by $\int_{-\infty}^{\chi} R / \int_{-\infty}^{0} R$. The probability is then assigned the same sign as that of the associated χ. The resolution function is:

$$R(-|\chi|) = -p_1 \cdot \chi \cdot e^{-.5(\chi/p_2)^2} + p_3 \cdot e^{\chi/p_4} + p_5 \cdot e^{\chi/p_6} + p_7 \cdot \chi \cdot e^{-.5(\chi/p_8)^2}$$

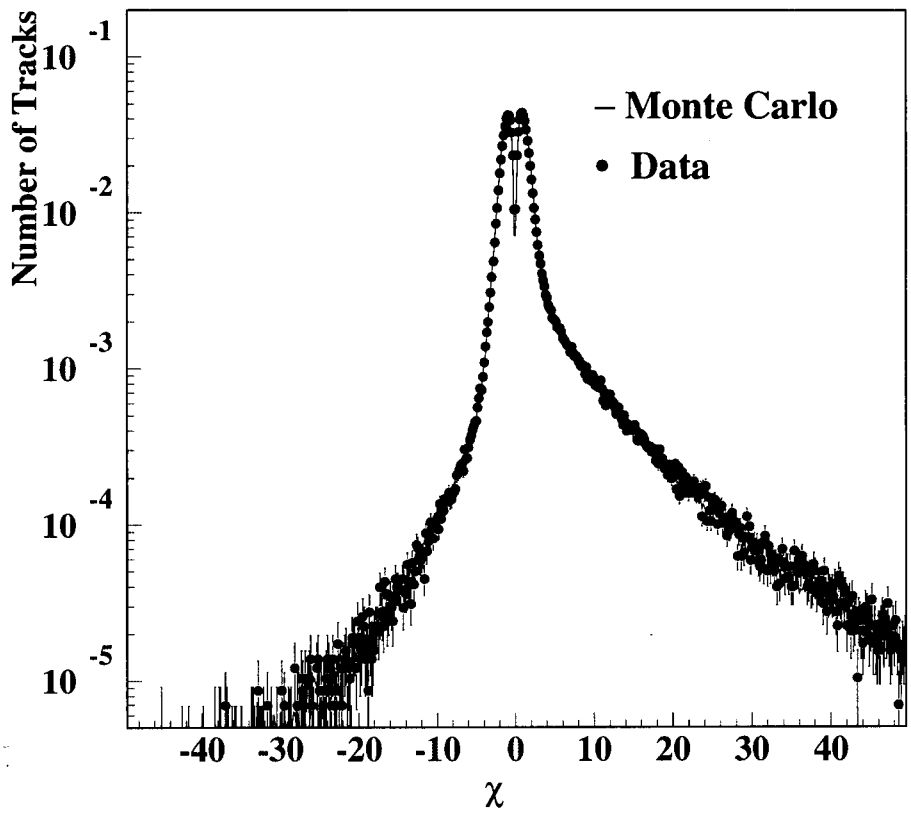

Figure 2: Data and Monte Carlo distributions of χ.

where the p_i variables are the parameters that are fitted. The $-\chi$ distribution for light quark events along with the fitted resolution function is shown in Fig. 4. The distributions of the probabilities for the tracks are shown in Fig. 5. Since the probabilities are derived from the *uds* distribution one expects the probability distribution for *uds* events to be flat; in sharp contrast, the tracks from *b* events exhibit a large peak near low probability for being consistent with the primary vertex. This is due to tracks from the *b*-decay vertex that have large impacts with respect to the primary vertex. The tails are due to fragmentation tracks.

The probability that the group of tracks belonging to a hemisphere are consistent with coming from the primary vertex is formed from the product of the positive track probabilities within the hemisphere ($P_{hemi} = \prod_{j=0}^{N_{tracks}} P_{track}^{j}$). From this the integral probability which expresses the chance that a larger χ^2 corresponding to the set of tracks would be measured is calculated. Since one is dealing with small samples, the Poisson χ^2 probability distribution[10] is used:

$$P(\chi^2|\nu) = e^{-\frac{\chi^2}{2}} \sum_{j=0}^{\frac{\nu}{2}-1} \frac{\frac{\chi^2}{2}^j}{j!}$$

where $\chi^2/2 = -ln(P_{hemi})$ and ν is the number of degrees of freedom. For each track there are two degrees of freedom ξ and η. Putting in the values for χ^2 and ν one gets:

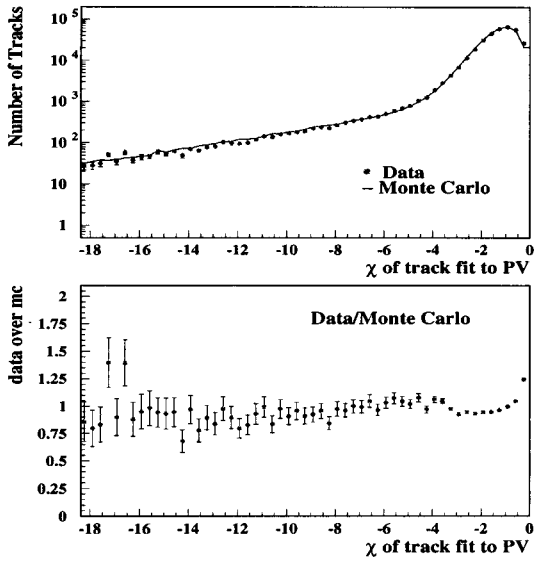

Figure 3: Comparison of the 3-D significance variable χ between data and Monte Carlo for tracks whose point of closest approach to the jet access is behind the primary vertex. Efficiency and minor resolution corrections have been applied.

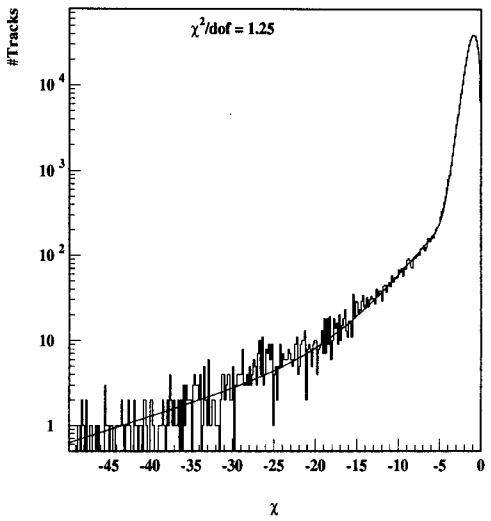

Figure 4: Negative χ distribution for tracks in *uds* events overlayed with the fit of the resolution function.

$$\Pi_{hemi} = \left(\prod_{j=0}^{n} P^j_{track}\right) \sum_{k=0}^{n-1} \frac{\left(-ln\left(\prod_{j=0}^{n} P^j_{track}\right)\right)^k}{k!}$$

The distribution of these hemisphere probabilities for different flavor events in the Monte Carlo are shown in Fig. 6. As lower probability cuts are required the b content of the tagged sample is greatly enhanced relative to the other flavors. Note that on the scale of $-ln(\Pi_{hemisphere})$, as one goes to higher values (to the right) one is requiring that the tracks in the hemisphere be less likely to be consistent with the primary vertex.

4.3 Determining R_b from Tag Counts

A hemisphere is tagged by requiring that the probability for the hemisphere $\Pi_{hemi} < P_{cut}$. In the analysis the number of hemisphere tagged (single tags) and number of events with both hemispheres tagged (double tags) are used to simultaneously measure ϵ_b and R_b. As with the derivation of R_b from the event tag one begins by expressing the net tag count in terms of the efficiencies for each of the flavor samples and the number of events in the untagged sample. The number of tagged hemispheres is given by:

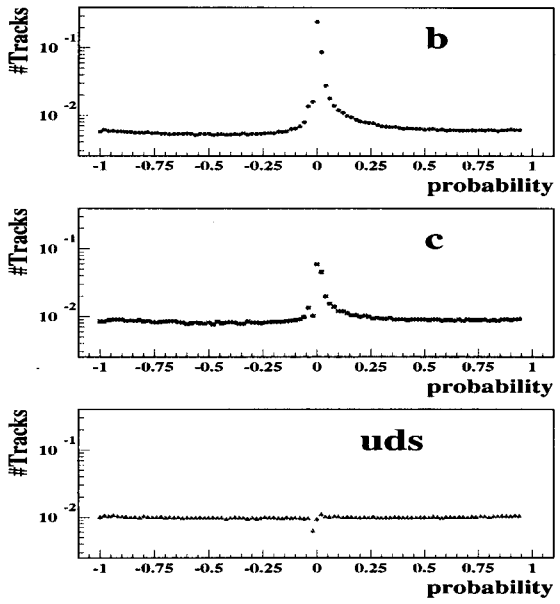

Figure 5: Distribution of tracks probabilities for consistency with coming from the primary vertex for b, c and uds events.

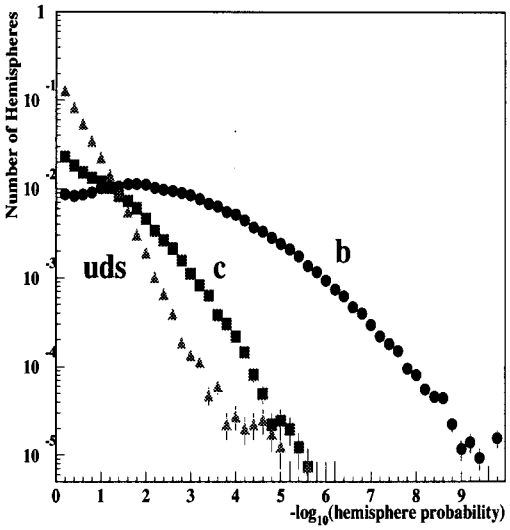

Figure 6: Distribution of hemisphere probabilities for b, c and uds flavored events.

$$n_{hemi} = \epsilon_b n_b + \epsilon_c n_c + \epsilon_{uds} n_{uds} \tag{2}$$

There is an additional equation for the tag count for the case where both hemispheres are tagged with the corresponding efficiencies for tagging both hemispheres as a function of the flavor. The number of double tagged hemisphere is given by:

$$n_{double} = \epsilon_b^{double} n_b + \epsilon_c^{double} n_c + \epsilon_{uds}^{double} n_{uds} \tag{3}$$

If no correlation existed between the hemispheres then $\epsilon_i^{double} = \epsilon_i^2$. The degree of correlation between the hemisphere should express the difference between these two quantities. The correlation, λ, is derived from the standard formula:

$$\lambda = \frac{< xy > - < x >< y >}{\sqrt{(< x^2 > - < x >< x >)(< y^2 > - < y >< y >)}}$$

with the variables x and y being $\Theta\left(P_{cut} - P\right)$ (i.e. 1 if the hemisphere passes the tag, 0 otherwise) for the first and second hemispheres respectively. The average of either variable (x or y) is the hemisphere tagging efficiency. The same is true for the square of the variables. The average of the product of the variables is the double hemisphere tagging efficiency. Thus, one gets:

$$\lambda_q = \frac{\epsilon_q^{double} - \epsilon_q^2}{\epsilon_q - \epsilon_q^2}$$

The terms in Eqn. 2 and 3 for the tag count can be rearranged so that everything is expressed in terms of the single hemisphere tag efficiencies and the correlation. Due to the low efficiency for tagging c and uds events and since the hemisphere correlations will be small, the λ_c and λ_{uds} are second order terms that may be dropped. The expression for the number of double tagged events is then:

$$n_{double} = (\epsilon_b^2 + \lambda_b(\epsilon_b - \epsilon_b^2))n_b + \epsilon_c^2 n_c + \epsilon_{uds}^2(n_{hadrons} - n_b - n_c)$$

$R_b = \frac{n_b}{n_{hadrons}}$ can be solved for with the dependence on ϵ_b removed by combining the equations for the number of single hemisphere tags and double hemisphere tagged events. For R_b this yields:

$$R_b = \frac{(F_s - R_c(\epsilon_c - \epsilon_{uds}) - \epsilon_{uds})^2}{F_d - R_c(\epsilon_c - \epsilon_{uds})^2 + \epsilon_{uds}^2 - 2F_s\epsilon_{uds} - \lambda_b R_b(\epsilon_b - \epsilon_b^2)} \tag{4}$$

where $F_{s,d}$= fraction of hemisphere single(s) and event double(d) tags. For ϵ_b the corresponding equation is:

$$\epsilon_b = \frac{F_d - R_c\epsilon_c(\epsilon_c - \epsilon_{uds}) - F_s\epsilon_{uds} - \lambda_b R_b(\epsilon_b - \epsilon_b^2)}{(F_s - R_c(\epsilon_c - \epsilon_{uds}) - \epsilon_{uds}} \tag{5}$$

These equations are coupled through the correlation terms and must be solved iteratively.

To determine the inputs, a 2-D histogram of the $-log_{10}\Pi_{hemi}$ of one hemisphere versus the other for b, c and uds events and data are used to determine the single and double hemisphere tagging efficiencies and tagging fractions. For each of the systematics studied a corresponding set of 2-D histograms is used.

4.4 Statistical Uncertainties with Correlation Effects Included

Correlation contributions are included in the estimation of the statistical uncertainties. The tag counts are separated into three independent categories; the count of events with both hemispheres are tagged(n_2), only one is tagged(n_1), and where neither are tagged(n_0). The counts for each case are then varied by their statistical error and the corresponding tag fraction or efficiencies are recalculated. The resulting changes in R_b are combined in quadrature to obtain the R_b statistical uncertainty. The statistical uncertainties on R_b and ϵ_b^{data} are shown in Fig. 7 and Fig. 8 versus the hemisphere probability cut.

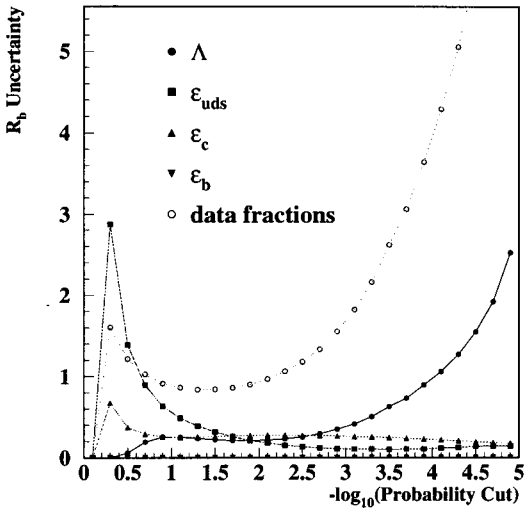

Figure 7: Statistical uncertainties in R_b.

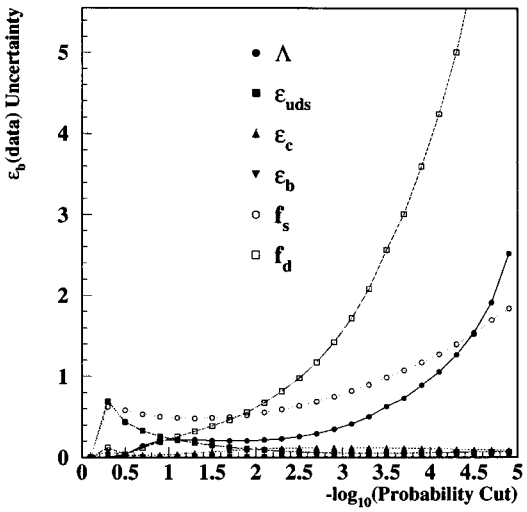

Figure 8: Statistical uncertainties in ϵ_b.

5 Measurement Results

The b-tagging purity(Π_b) versus ϵ_b performance of the b-tag is shown in Fig. 10. The b-tag performance for the hemispheres versus Π_{hemi} is shown in Fig. 9. Note that the estimated and measured b-tagging efficiencies agree well over the whole probability range. Deviations between these values would indicate either incorrect physics simulation or detector resolution simulation. These efficiencies along with the b-hemisphere correlations measured from the Monte Carlo and the single and double hemisphere tagging fractions in data collected from the 1993 and 1994 SLD runs yield the R_b values shown in Fig. 11. The results have been corrected for the event selection bias.

6 Systematics

The systematics come from correlation uncertainties, c tagging efficiency and uds tagging efficiency uncertainties. These systematics are described below:

6.1 Physics Systematics

- **Correlation Systematics**
  The b-physics systematics enter only indirectly through the correlation estimation since the b-tagging efficiency is simultaneously measured from the data. The variations applied to the B-simulation parameters to determine the systematics are shown in Table 2. The results are shown in Fig. 12.

- **Charm systematics**
  The variations applied to the charm physics modelling parameters are shown in

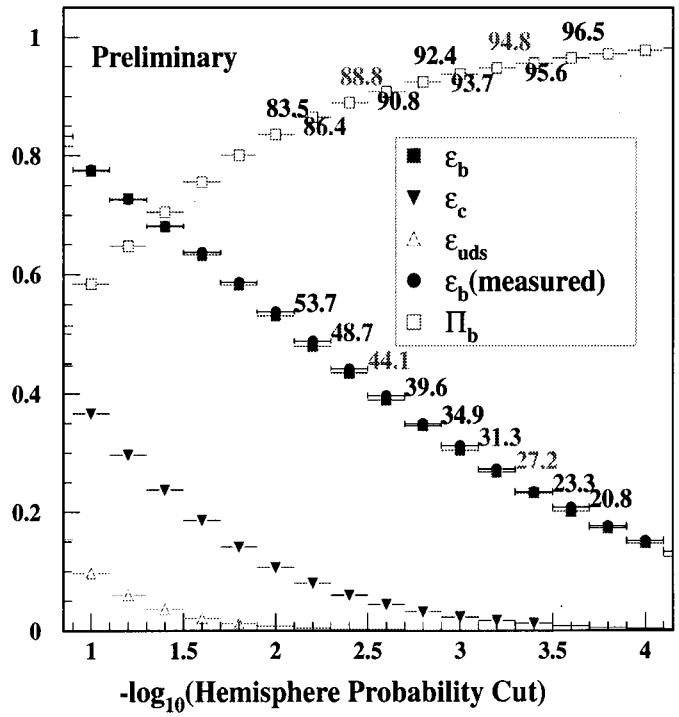

Figure 9: b-tag dependence on hemisphere probability cut.

B Physics Simulation Systematic	Variation Applied
B-lifetimes	$\tau_{Bmeson} = 1.55 \pm 0.10$ ps, $\tau_{Bbaryon} = 1.10 \pm 0.30$ ps
b-fragmentation	Peterson $\langle x_e \rangle = 0.695 \pm 0.021$
b-baryon production	$7.8 \pm 3.0\%$
B-decay to D^+	$\pm 6\%$ absolute
B-decay multiplicity	± 0.25 tracks per B decay

Table 2: Variations to B simulation parameters used to determine R_b systematics.

Table 3. As is shown in Fig. 12, the largest contribution to the total uncertainty comes from the estimation of the charm tagging efficiency. This is expected as it has the largest tagging efficiency not measured from the data. The largest contribution is from the uncertainty in the charm fragmentation. Comparable in magnitude to this is the rate at which D^+s are produced in c events relative to other charmed hadrons. As expected, the D^+ contribution dominates over the others due to is significantly longer lifetime.

- R_c
  There is a correlation of R_b with R_c of -0.11. The current uncertainty on R_c of 10% gives the systematic from R_c shown in Fig. 12.

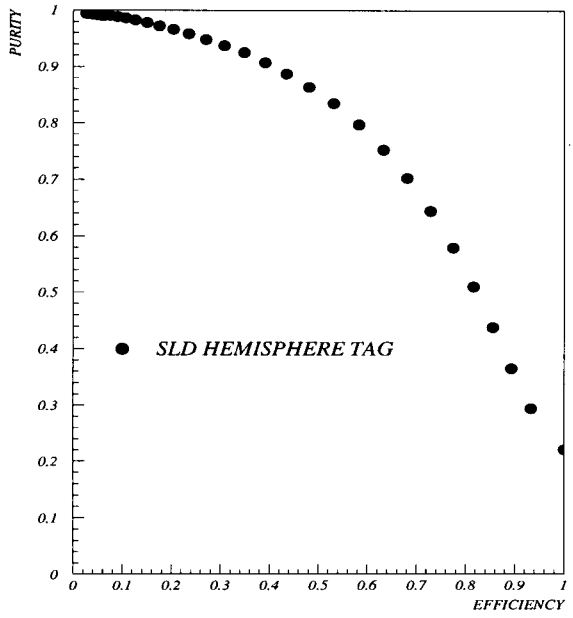

Figure 10: SLD b-tag performance.

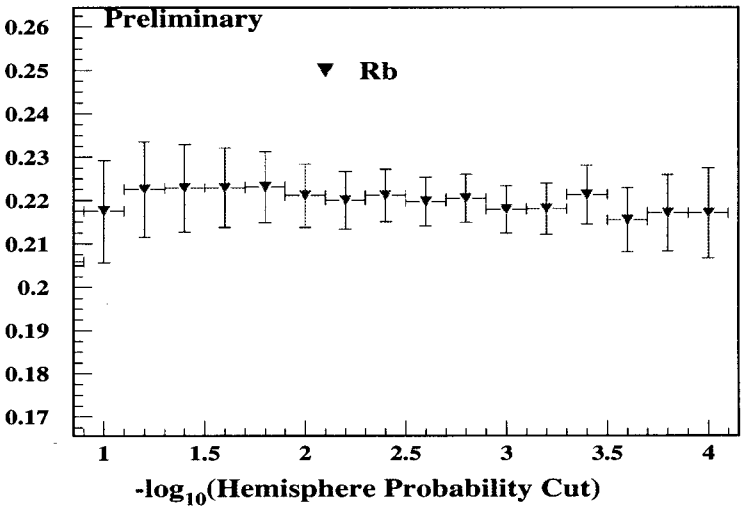

Figure 11: R_b from the lifetime probability tag versus the hemisphere probability cut.

- **Light Quark Systematics**
  As the efficiency for tagging light quarks is very small relative to ϵ_c the light quark systematic contributions are likewise small despite the factor of 3 greater production. The variations applied are shown in Table 3 and the resulting changes in R_b are shown in Fig. 12. All of the light quark systematics are well under 1%. Due to concern about the lack of knowledge about gluon splitting in light quark events and the potential sensitivity that this measurement might have to it the amount has been varied by 100%.

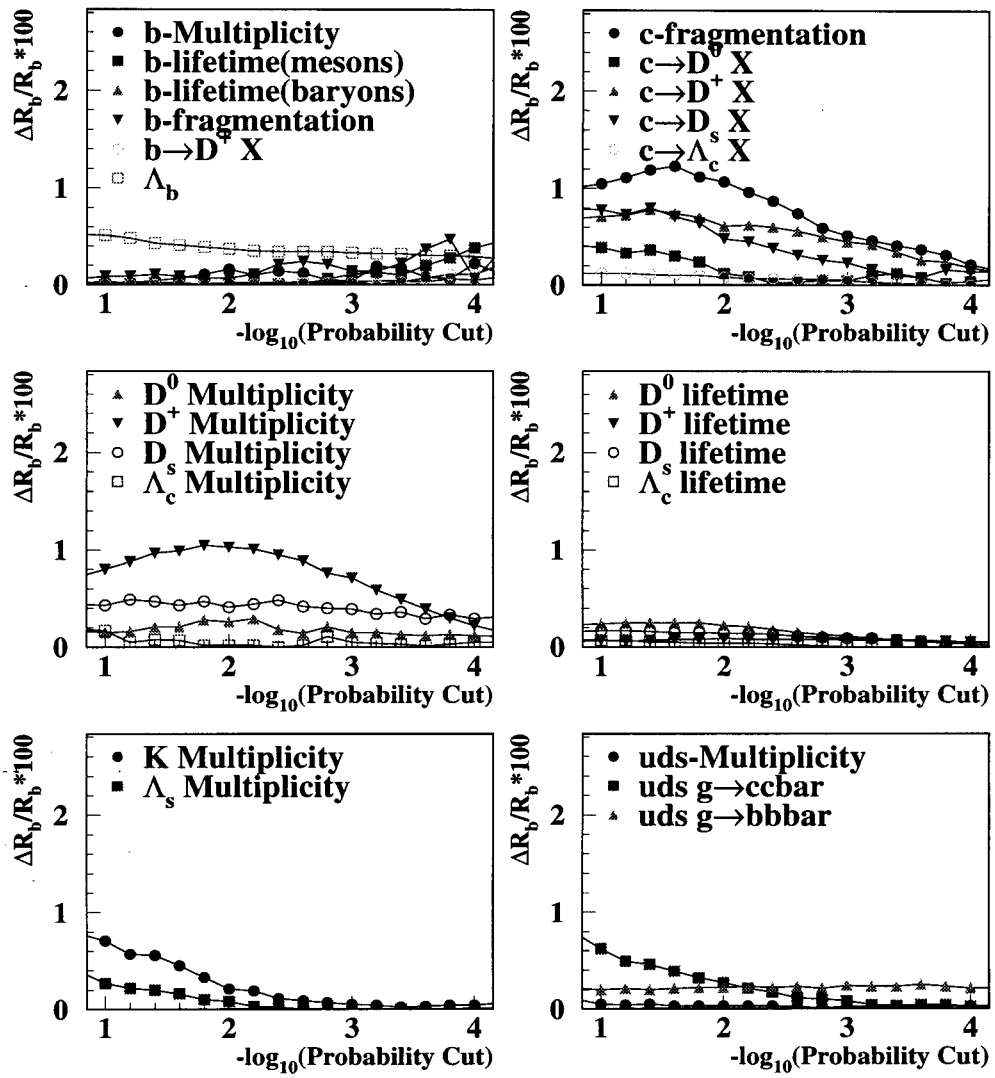

Figure 12: Physics contributions to the uncertainty in R_b versus the hemisphere probability cut.

6.2 Detector Systematics

The detector systematics include tracking efficiency and resolution corrections. The effects of these on R_b and ϵ_c are shown in Fig. 13 as a function of the hemisphere probability cut. Other contributions coming from tails on the primary vertex position measurement and from V^0 rejection are not included in this plot and are only given at the optimal probability cut.

- **Impact Resolution Systematics**
  The full amount of the change caused by the smearing corrections described in Sect. 3 is taken as the systematic. In Fig. 14 this uncertainty is shown as strongly decreasing with tighter cuts. This is due directly to the decrease in ϵ_c with tighter cuts.

Physics Systematic	Variation Applied
c-fragmentation	Peterson $\langle x_e \rangle for D^* = 0.501 \pm 0.025$
$c \to D$	D^0:±5.3%, D^+:±3.7%, D_s:±7.0%, Λ_c:±0.5%
c decay multiplicity	D^0:±0.06, D^+:±0.10, D_s:±0.31, Λ_c:±0.40
strange particle production	$s\bar{s}$ popping varied by 10%
***uds*-decay multiplicity**	±0.3 tracks
$g \to b\bar{b}$ **splitting**	±100%
$g \to c\bar{c}$ **splitting**	±100%
$\Gamma(Z^0 \to c\bar{c})$	$R_c = 0.171 \pm 0.017$

Table 3: Variations to the light quark decay simulation parameters used to determine R_b systematics.

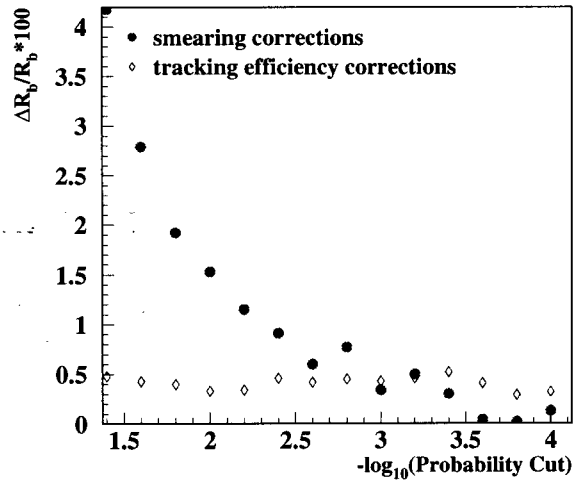

Figure 13: Uncertainties in R_b from efficiency and smearing corrections.

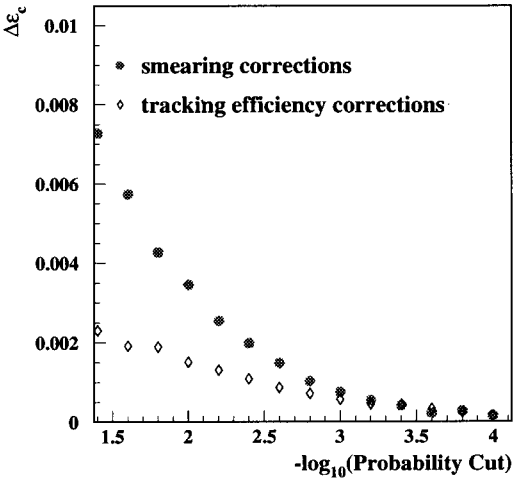

Figure 14: Uncertainties in ϵ_c from efficiency and smearing corrections.

- **Tracking Efficiency Corrections**
  To estimate the systematic error associated with the $p_\perp$, ϕ and $cos\theta$ dependence of the track efficiency corrections, the change in R_b when it is remeasured with these dependencies averaged out relative to the nominal R_b result is used. The resulting variations in R_b are summed in quadrature. The dominant contribution comes from the 0.4 track per event variation. The uncertainty in ϵ_c caused by the efficiency uncertainties is shown in Fig. 14.

- **Primary Vertex Position**
  The measurement was repeated with the non-Gaussian primary vertex position tails added as described in Ref. [4]. At the optimal cut of $10^{-3.0}$ the resulting variation is 0.3% and is taken as the systematic.

- **V^0 rejection**
  The measurement was reperformed with the V^0 rejection removed. At the

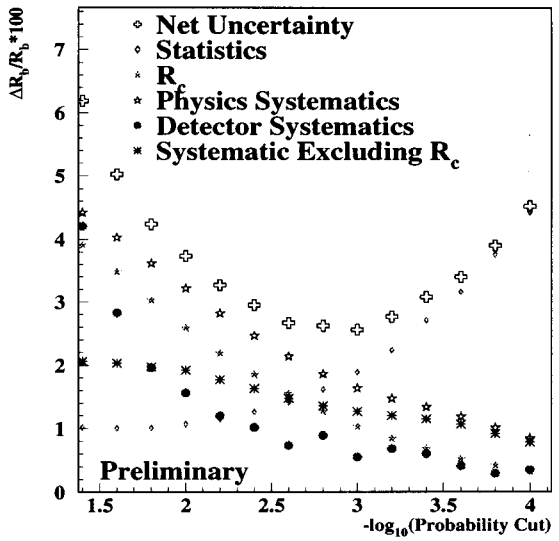

Figure 15: R_b systematic uncertainties versus hemisphere probability cut.

optimal cut of $10^{-3.0}$ the total change was 0.9%.

A general feature of all of the physics and smearing systematics is that they decrease with tighter tagging requirements. What prevents one from using a very tight cut are the contributions from the statistical uncertainties. This is promising as it implies that with more data both statistics and systematics will decrease as one can move towards tighter cuts. An optimal set of cuts having the highest combined (statistical plus systematic) precision can always be found.

6.3 Verifications

The result is checked for sensitivity to cuts, consistency between inputs from the individual data taking periods used, and any geometrical effects. Furthermore, attempts at independently determining the contributions to the correlation systematics are made.

6.3.1 Sensitivity to Cuts

Variations in the R_b result versus the probability cut would indicate simulation problems. Deviations from the central at low probability cuts would suggest a problem with the charm or detector simulation. Deviations at high probability cuts would suggest problems with the tracking efficiency simulation. As can be seen from Fig. 11 no significant deviations outside of the statistical plus systematic error bars are observed.

The significance variable χ is checked for any unsimulated variations as function of position within the detector. Such variations can cause contributions to the correlation. For example, in symmetric inefficiencies the jets from both quarks may have tracks in inefficient regions causing a positive correlation contribution. No aberrations are observed.

6.3.2 Correlation Components

The correlation between the b-hemispheres results from both physics and detector effects. The correlation between the b-hemispheres is shown versus the hemisphere probability cut in Fig. 16. It is desirable to isolate the contributions to the correlation so that it is known that all contributions to the systematic have been accounted for and not duplicated. A method has been developed whereby components of the correlation may be projected out[9]. The method involves determining how much of an influence tagging in one hemisphere as a function of some variable ν has on the distribution of ν in the other hemisphere. To calculate the correlation the distribution of the efficiency as a function of ν is convoluted with the distribution of ν, $h(\nu)$ in a hemisphere after the other hemisphere has been tagged as shown in Eqn. 6. Effectively, the correlation component is a measure of the probability that if a hemisphere has a value ν that is in a high(low) tagging efficiency region the other hemisphere is also in a high(low) tagging efficiency region.

$$\epsilon_\nu = \int \epsilon(\nu) h(\nu) d\nu \tag{6}$$

The influenced distribution $h(\nu)$ is determined from the convolution of the histogram $(H(\nu_1, \nu_2))$ containing b event counts versus ν_{hemi1} and ν_{hemi2} with the efficiency, ϵ_ν

$$h(\nu) = \sum_{\nu_1} H(\nu_1, \nu_2) \cdot \epsilon(\nu_1) \tag{7}$$

The double tag efficiency is then $\epsilon \times \epsilon_\nu$ thus the correlation component is:

$$\lambda_\nu = \frac{\epsilon \cdot \epsilon_\nu - \epsilon^2}{\epsilon - \epsilon^2} \tag{8}$$

Ideally, if all of the component have been identified then the sum of all of the components will add to the total correlation. It is necessary to insure that the components are independent. The components that have been studied are the $cos\theta$ of the quark direction, the ϕ of the quark direction, the momentum of the quark, the deviation of the $r\phi$ and rz of the beam position used from the true beam position, the B-lifetime and the B-momentum sum.

In Fig. 17 the distributions used to calculate a component of the correlation are shown. In this case ν is $cos\theta$. The top left plot shows the distribution of ν over

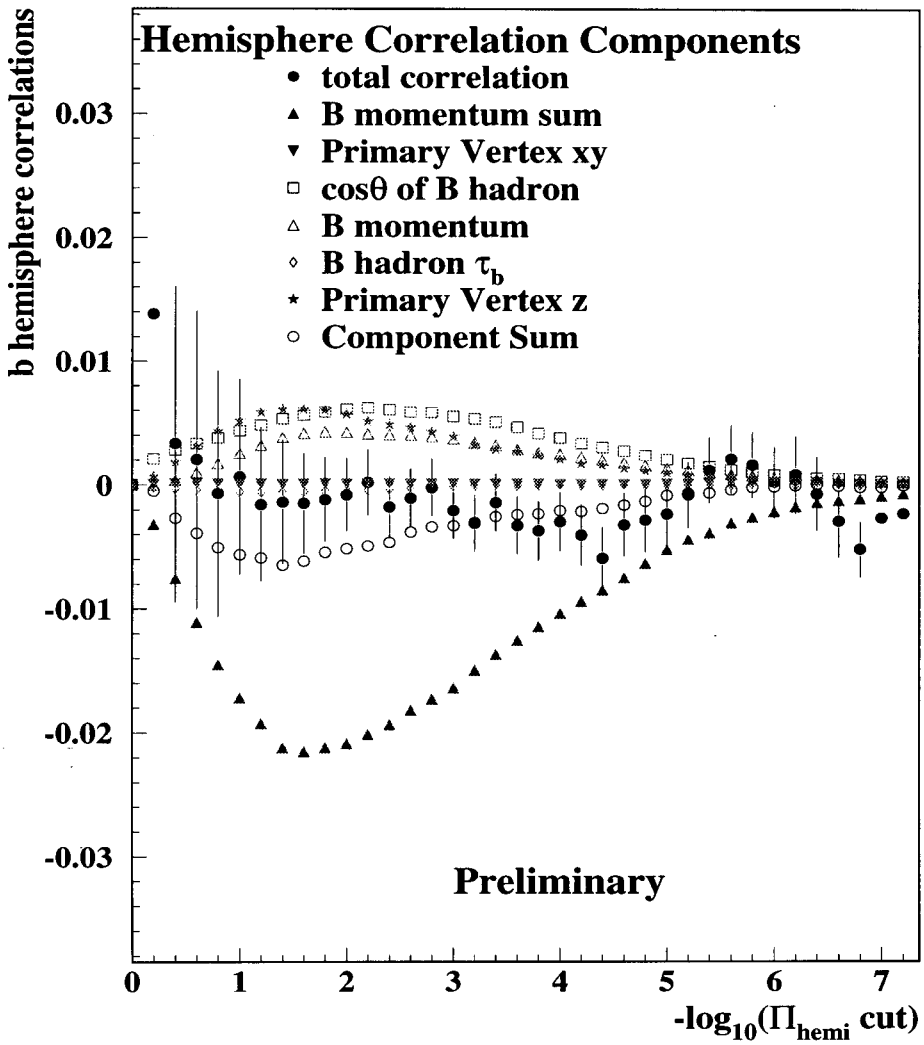

Figure 16: b-hemisphere correlation components.

the full range of the variable. Next, is shown the b-hemisphere tagging efficiency versus ν. The distribution of ν(the line) for tagged hemispheres compared to the distribution $h(\nu)$ obtained after the other hemisphere has been tagged is shown. If no correlation between the hemispheres existed then the distributions would be identical. In this case the convolution of $\epsilon(\nu)$ and $h(\nu)$ would yield the b-hemisphere tagging efficiency, ϵ. As can be seen from equation 8 this would result in $\lambda_\nu = 0.$. Finally the ratio of the influenced distribution to the original distribution is shown to clarify the ν dependence of the correlation. The distributions are for a cut of $\Pi_{hemi} = 10^{-2.0}$ which was chosen because the correlation components are large at this cut.

- **$cos\theta$ component**
  Correlations in $cos\theta$ are expected due to the back to back nature of the quark jets. If one jet points in a direction of low tagging efficiency so should the other thus a positive correlation should be observed.

- **ϕ component**

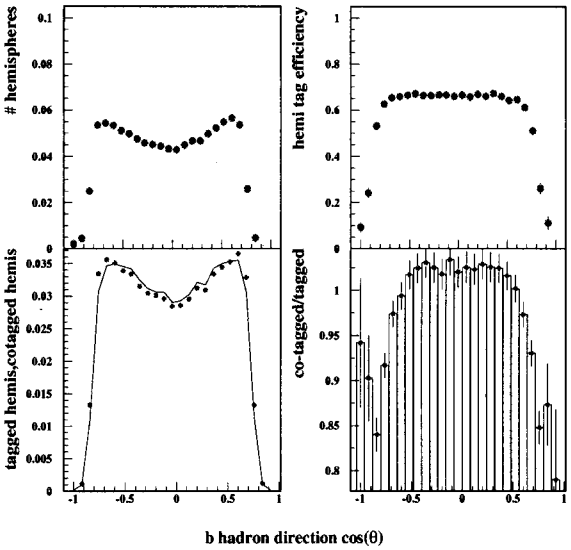

Figure 17: Distributions used to determine component of the correlation from the polar angles of the B-hadrons.

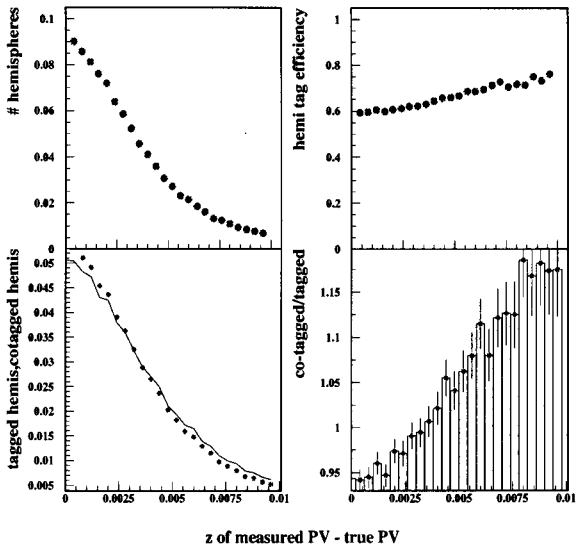

Figure 18: Distributions used to determine primary vertex z correlation component.

No correlation in ϕ is expected as the detector is nearly axially uniform. It is both a check for whether an error is causing a correlation to be seen where there isn't one and any unexpected detector defects. No correlation in the ϕ component is observed.

- **components from poorly measured beam positions**
  Poor beam position measurements can lead to both quarks going into the same hemisphere which would give a negative correlation and can also cause the probability for tracks in both hemisphere to be consistent with the primary vertex to be low thus causing both to tag and a positive correlation. This is clearly seen for the dependence on the longitudinal position shown in Fig. 18.

- **B-lifetime component**
  Theoretically, there is not an obvious means by which the lifetime of the hadrons in the separate hemispheres may communicate with each other except through erroneous beam positions. Since the τ_B influence on the resolution of the primary vertex position is small for SLD, this component is expected to be small. At the cut for which the result is given, this correlation is negligible.

- **B-momentum sum**
  The B-momentum sum variable is designed to account for gluon activity in the event. The variable is chosen to be:

$$\nu = \frac{(\vec{P}_B + \vec{P}_{\overline{B}}) \cdot \hat{H}}{|\vec{P}_B + \vec{P}_{\overline{B}}|} \tag{9}$$

where $\hat{H}$ is the axis for the corresponding hemisphere. In the case where both B's go into the same hemisphere the value of $|\nu|$ will be large and the hemisphere

for which it is positive should have a high probability of tagging while the other has a negligible chance of being tagged. The result is a negative correlation between the hemispheres.

- **B-momentum**
  The B-momentum measures correlations from the fragmentation process. Here, the variable ν is the momentum of the B-hadron for each hemisphere when they have gone into separate hemispheres.

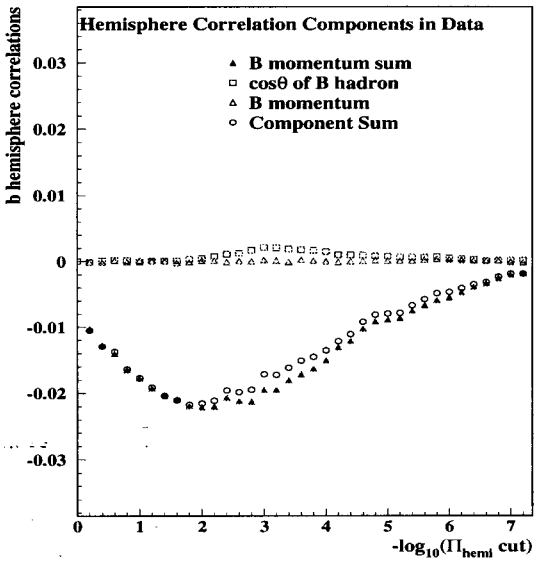

Figure 19: Correlation components estimated from the data.

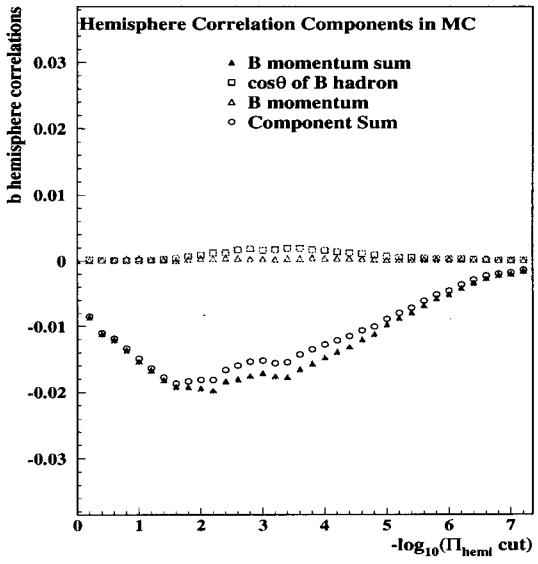

Figure 20: Correlation components estimated from the Monte Carlo.

The total correlation along with its components are shown in Fig. 16. The majority of the components show a positive correlation between the hemispheres. These are balanced by the large negative component from the gluon activity represented by the B-momentum sum.

The total correlation and the sum of the correlation components are consistent within errors. Thus, there is no evidence that any large unexpected systematics entering through the correlation exist. These tests have been performed using only the Monte Carlo. A check of the correlation simulation was performed as described in the following section.

6.4 Check of correlation components from data

An approximation of the correlation components is obtained from the data. The truth information for the B-hadron directions is replaced with the directions of the highest momentum jets and the true B-hadron momenta are replaced with the momenta of the jets. With these replacements the correlations can be determined from the data and may be compared to those obtained from a properly flavor mixed Monte Carlo

sample. To reduce the contamination from light quark events, events are required to have at least three tracks with 3-D impact parameter significance greater than 3.0. The b-efficiency of this event tag is 72% and the b-purity is 85%. The resulting correlation components are shown in figures 19 and 20. Certain correlations such as the displacement of the measured from the true primary vertex positions could not be approximated. Also, the $cos\theta$ correlation is reduced by performing the event tag. However, the expected features are seen. The $cos\theta$ component is positive and larger than the B-momentum component and the gluon activity from the B-momentum sum appears to be the largest contributor to the correlation.

The Monte Carlo appears to underestimate the gluon activity by -3%. Increasing the true B-momentum sum correlation by 3% causes a change in the correlation sum of 1.6×10^{-4}. The change in R_b from this variation in the correlation is 0.3%.

6.5 Summary of Systematics

The curves showing all detector, physics and R_c systematic and statistical uncertainties are displayed in Fig. 15. The contributions from the systematics on ϵ_c cause greater uncertainty at looser tag cuts while the statistical uncertainties start to dominate for tighter cuts. The minimum combined systematic occurs at $-log_{10}\Pi_{hemi} = 10^{-3.0}$. At this cut the combined uncertainty from all sources is $\delta R_b = 2.7\%$.

7 Final Result

The measurement of R_b is made at the point which minimizes the combined statistical plus systematic uncertainties. This occurs at the cut of $P_{cut} = 10^{-3.0}$. After applying all efficiency and resolution corrections and correcting for biases introduced by the event selection, the results shown in Tables 4, 5 and 6 are obtained with the final result for R_b from the probability tag being

$$R_b = 0.2171 \pm 0.0040_{statistical} \pm 0.0037_{systematic} \pm 0.0023_{R_c} \quad (preliminary) \qquad (10)$$

Monte Carlo Measurements	
ϵ_b	30.6%
Π_b	94 %
b hemisphere correlation	-0.21%
ϵ_c	2.3%
ϵ_{uds}	$(8.7 \cdot 10^{-2})\%$

Data Measurements	
ϵ_b	$(31.3 \pm 0.6)\%$
F_s	7.4%
F_d	2.2%

Table 4: Probability tag performance for $P_{cut} = 10^{-3.0}$.

At the current precision, the SLD result is consistent with LEP's R_b result as well as the Standard Model prediction for R_b. Significant improvements in the precision of the SLD measurement will result from data(0.5 M Z^0) to be collected in the scheduled runs ahead with the new SLD vertex detector.

Correlation Systematics			
Systematic	$\delta R_b/R_b$	Systematic	$\delta R_b/R_b$
τ_B	<0.1%	B-decay multiplicity	0.1%
$B \to D$	<0.1%	b fragmentation	0.3%
Λ_b fraction	0.3%	MC statistics	0.4%
Charm Systematics			
Systematic	$\delta R_b/R_b$	Systematic	$\delta R_b/R_b$
$c \to D^0$	<0.1%	$c \to D^{\pm}$	0.5%
$c \to D_s$	0.3%	$c \to \Lambda_c$	<0.1%
D^0 multiplicity	0.2%	$D^{\pm}$ multiplicity	0.7%
D_s multiplicity	0.4%	Λ_c multiplicity	0.1%
D^0 lifetime	0.1%	$D^{\pm}$ lifetime	0.1%
D_s lifetime	0.1%	Λ_c lifetime	<0.1%
c fragmentation	0.6%	R_c	1.1%
MC statistics	0.3%		
Light Quark Systematics			
Systematic	$\delta R_b/R_b$	Systematic	$\delta R_b/R_b$
K production	0.1%	Λ_s production	<0.1%
$g \to c\bar{c}$	<0.1%	$g \to b\bar{b}$	0.2%
MC statistics	0.1%		

Table 5: Summary of physics systematics for probability tag at a cut of $P_{cut} = 10^{-3.0}$

Detector Systematics			
Systematic	$\delta R_b/R_b$	Systematic	$\delta R_b/R_b$
Efficiency Corrections	0.4%	V^0 Rejection	0.9%
Impact Resolutions	0.4%	Beam Position Tails	0.3%

Table 6: Summary of detector systematics for probability tag at a cut of $P_{cut} = 10^{-3.0}$

References

[1] G. Park, *Implication of the Recent Top Quark Discovery on Two Higgs Doublet Model*, **HEP-PH-9504369**, (1995).

[2] S. Abachi *et. al.*, *Observation of the Top Quark*, **HEP-EX-9503003**, (1995).

[3] J. Liu and D. Ng, *The effect of new physics on R_b*, **TRI-PP-94-71**, (1994).

[4] K. Abe *et. al.*, *Measurements of R_b using Impact Parameters and Displaced Vertices*, **SLAC-PUB-95-6569**, (1995).

[5] M. Hildreth *et. al.*, **SLAC-PUB-6656** *Submitted to IEEE Trans. on Nucl. Sci.* (1994).

[6] G. Agnew *et. al.*, **SLAC-PUB-5906** *Proceedings of the 26th International Conference on High Energy Physics, Dallas, Texas, USA, Aug 1992.*

[7] D. Axen *et. al.*, *Nucl. Instr. & Meth.* **A328**, 472 (1993).

[8] SLD Collaboration: G. Agnew *et. al.*, *SLD Design Report* **SLAC-0273** (1984).

[9] ALEPH Collaboration: D. Buskulic *et. al*, *Phys.Lett.* **B313**, 535 (1993);
OPAL Collaboration: P. D. Acton *et. al*, *Z. Phys.* **C60**, 579 (1993);
OPAL Collaboration: D. Akers *et. al*, *Z. Phys.* **C65**, 17 (1994);
DELPHI Collaboration: P. Abreu *et. al*, *Z. Phys.* **C65**, 555 (1995).

[10] M. Abramowitz and I. Stegun, *Handbook and Mathematical Functions*, 941 (1972).